arXiv:1604.06449v1 [cond-mat.str-el] 21 Apr 2016

Critical local moment fluctuations and enhanced pairing correlations in a cluster Anderson model

Ang Cai,[1] J. H. Pixley,[2] Kevin Ingersent,[3] and Qimiao Si[1]

[1] *Department of Physics and Astronomy, Rice University, Houston, Texas, 77005, USA*
[2] *Condensed Matter Theory Center and the Joint Quantum Institute, Department of Physics, University of Maryland, College Park, Maryland 20742-4111, USA*
[3] *Department of Physics, University of Florida, Gainesville, Florida 32611-8440, USA*

(Dated: April 22, 2016)

The appearance of unconventional superconductivity near many heavy-fermion quantum critical points (QCPs) motivates investigation of pairing correlations close to a "beyond Landau" Kondo-destruction QCP. We focus on a two-Anderson-impurity cluster in which Kondo destruction is induced by a pseudogap in the conduction-electron density of states. Analysis via continuous-time quantum Monte-Carlo and the numerical renormalization group reveals a previously unstudied QCP that both displays the critical-local moment fluctuations characteristic of Kondo destruction and leads to a strongly enhanced singlet-pairing susceptibility. Our results shed light on the extent to which different kinds of magnetic interactions induce pairing correlations in non-Fermi liquid settings, thereby providing new insights into the mechanism for unconventional superconductivity in quantum critical metals.

PACS numbers: 71.10.Hf, 71.27.+a, 74.40.Kb, 74.70.Tx, 75.20.Hr

Heavy-fermion metals represent a prototype system in which unconventional superconductivity is driven by antiferromagnetic correlations [1, 2]. Experiments on these strongly correlated systems have revealed quantum criticality in a wide range of compounds. Detailed theoretical and experimental studies have provided evidence for different classes of quantum critical point (QCP). One class follows the Landau theory, in which criticality is dictated by the fluctuations of an order parameter. Here, the broken-symmetry state is a spin density wave, and the theoretical description starts from the spatial and temporal fluctuations of the antiferomagnetic order parameter [3–5].

Another class of QCP goes beyond the Landau framework, in that it involves new critical modes besides order-parameter fluctuations. The additional critical modes describe a critical destruction of the Kondo entanglement between the localized magnetic moments and conduction electrons [6, 7]. An important example of a Kondo-destruction QCP occurs in $CeRhIn_5$, which has the highest T_c among all the Ce-based heavy-fermion superconductors [8–11] and is generally believed to have a $d_{x^2-y^2}$ superconducting gap symmetry. A sudden change of the Fermi-surface topology at the antiferromagnetic QCP in $CeRhIn_5$, accompanied by a diverging tendency of the carrier effective mass [12], defy explanation within the spin-density-wave scenario for quantum criticality. Instead, these properties provide evidence supporting the Kondo-destruction picture.

How unconventional superconductivity arises near a Kondo-destruction QCP has yet to receive systematic theoretical study. The question is challenging because the normal state is a non-Fermi liquid with Landau quasiparticles turned critical. It has previously proved illuminating to study the notion of Kondo destruction within quantum impurity models [13–17]. Indeed, the QCP in the single-impurity pseudogap Kondo and Anderson models captures similar critical properties to the Kondo-destruction QCP in the lattice problem (as solved within an extended dynamical mean field theory [6]), including a vanishing Kondo energy scale, ω/T scaling of the dynamics, and a fractional exponent in the temperature dependence of the local spin susceptibility. However, due to its single-site nature, a single-impurity model is not suitable for studying unconventional non-local pairing. An avenue for addressing this important issue has been opened by the development of a cluster extended dynamical mean-field theory (C-EDMFT) [18], which maps the periodic Anderson model to a quantum cluster model coupled to self-consistently determined fermionic and bosonic baths, where the latter decoheres and eventually destroys the Kondo entanglement [19].

The logical first step toward the full C-EDMFT treatment of pairing correlations near a Kondo-destruction QCP is to study the corresponding properties in non-self-consistent quantum cluster models. Recent work [20] has shown enhanced pairing correlations in an Ising-anisotropic two-impurity Bose-Fermi Anderson model where the mechanism for Kondo destruction is the coupling of the z components of the impurity spins to a bosonic bath. This finding raises two important questions: Does Kondo-destruction quantum criticality robustly promote superconducting pairing correlations? If so, what types of interaction are important?

In this work we study a two-impurity pseudogap Anderson model with Ising exchange between the impurity spins, where the driving force for Kondo destruction—the exchange coupling of the impurity spins to a conduction

band with a density of states that vanishes in power-law fashion at the Fermi energy—preserves SU(2) symmetry. On general grounds, we can postulate that spin-isotropic magnetic interactions, which promote spin-singlet formation, would further boost the enhancement of pairing correlations. We will demonstrate that this indeed is the case for the Kondo-destruction QCP in the two-impurity pseudogap Anderson model when compared with the Ising-anisotropic two-impurity Bose-Fermi Anderson model.

Model and solution methods: The two-impurity Ising-anisotropic Anderson Hamiltonian is

$$H = \sum_{\mathbf{k},\sigma} \epsilon_{\mathbf{k}}\, c^\dagger_{\mathbf{k}\sigma} c_{\mathbf{k}\sigma} + \frac{V}{\sqrt{N_k}} \sum_{\mathbf{k},j=1,2,\sigma} \left(e^{i\mathbf{k}\cdot\mathbf{r}_j} d^\dagger_{j\sigma} c_{\mathbf{k}\sigma} + H.c. \right) + \sum_{j=1,2,\sigma} \epsilon_d\, d^\dagger_{j\sigma} d_{j\sigma} + \sum_{j=1,2} U n_{j\uparrow} n_{j\downarrow} + I_z S^z_1 S^z_2, \qquad (1)$$

with $\epsilon_{\mathbf{k}}$ being the conduction-electron dispersion, V the hybridization (assumed to be local), N_k the number of unit cells in the host, ϵ_d the impurity level energy, U the on-site repulsion, and I_z the Ising exchange coupling between the impurities at positions $\mathbf{r}_1$ and $\mathbf{r}_2$; $S^z_j = \sum_{\alpha,\beta} d^\dagger_{j\alpha} \frac{1}{2} \sigma^z_{\alpha,\beta} d_{j\beta}$, where $\sigma^z_{\alpha,\beta}$ is the Pauli matrix. The conduction-band density of states is chosen to be

$$\rho(\epsilon) = \frac{1}{N_k} \sum_{\mathbf{k}} \delta(\epsilon - \epsilon_{\mathbf{k}}) = \rho_0 |\epsilon/D|^r\, \Theta(D - |\epsilon|), \qquad (2)$$

where D is the half-bandwidth. For $r > 0$, $\rho(\epsilon)$ has a pseudogap at the Fermi energy ($\epsilon = 0$). The impurity-band coupling is fully specified by the hybridization function $\Gamma(\epsilon) = \pi \sum_k V^2 \delta(\epsilon - \epsilon_k) = \Gamma_0 |\epsilon/D|^r$ with hybridization width $\Gamma_0 = \pi \rho_0 V^2$.

For simplicity, we consider only the particle-hole-symmetric case $\epsilon_d = -U/2$ and take the limit of infinite separation $|\mathbf{r}_1 - \mathbf{r}_2|$ in which there is a vanishing hybridization-induced Ruderman-Kittel-Kasuya-Yosida interaction and the two impurities are coupled only via the Ising exchange I_z. With $I_z = 0$, we have two independent one-impurity pseudogap models; for $0 < r < \frac{1}{2}$, a Kondo-destruction QCP [21] that we denote CR1 separates a Kondo phase ($\Gamma_0 > \Gamma_c$) from a local-moment phase ($\Gamma_0 < \Gamma_c$). With $\Gamma_0 = 0$ and $I_z > 0$, the two impurity spins are decoupled from the conduction band and anti-align in an Ising antiferromagnetic configuration. Our goal is to probe the quantum phase transitions that arise when both $\Gamma_0 > 0$ and $I_z > 0$ [22].

We can begin by analyzing the perturbative effect of the coupling I_z near the single-impurity critical point CR1. At this QCP, $\langle S^z_i(\tau) S^z_i \rangle \sim \tau^{-(1-x_1)}$, with x_1 being an r-dependent exponent that satisfies $0 < x_1(r) < 1$ [16]. Since the impurities decouple, $\langle S^z_1(\tau) S^z_2(\tau) S^z_1 S^z_2 \rangle \sim \tau^{-2(1-x_1)}$. The scaling dimension of $S^z_1 S^z_2$ is thus seen to be $1 - x_1(r)$ and we obtain the scaling dimension $[I_z] = x_1(r)$. The Hamiltonian term $I_z S^z_1 S^z_2$ is therefore

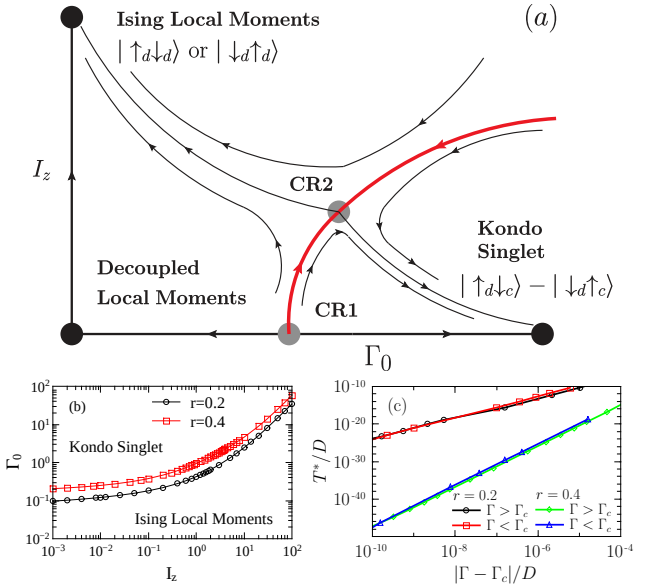

FIG. 1. (a) Conjectured RG flow of the symmetric two-impurity pseudogap Anderson model. Gray dots represent unstable fixed points and black dots represent stable fixed points. CR1 is the unstable fixed point of the single-impurity pseudogap Anderson model. CR2 is the unstable fixed point of the two-impurity model studied in this work. The red line marks the separatrix and phase boundary. (b) Phase boundary of the symmetric two-impurity pseudogap Anderson model on the I_z–Γ_0 plane for $r = 0.2$, $U = -2\epsilon_d = 0.3$ and for $r = 0.4$, $U = -2\epsilon_d = 0.1$. The boundary value of Γ_0 obtained from NRG calculations is plotted before extrapolation to the continuum limit [27]. (c) Crossover scale T^* from the NRG vs $|\Gamma_0 - \Gamma_c|$ on both sides of the phase boundary for $r = 0.2$, $I_z = 1.54$, $\Gamma_c \simeq 0.5503$ and for $r = 0.4$, $I_z = 0.73$, $\Gamma_c \simeq 0.8032$. Fits to $T^* \propto |\Gamma_0 - \Gamma_c|^\nu$ yield estimated exponents given in the text.

a relevant perturbation at CR1 and will likely lead the two-impurity model to a new unstable fixed point CR2 as shown on a conjectured RG flow diagram in Fig. 1(a).

Since the pseudogap breaks conformal invariance, the model (1) cannot be treated nonperturbatively using conventional analytical methods and we instead employ continuous-time quantum Monte-Carlo (CT-QMC) [23, 24] and the numerical renormalization group (NRG) [25, 26]. We present results for two representative cases: (i) $r = 0.2$, $U = 0.3$ and (ii) $r = 0.4$, $U = 0.1$, where we have set the energy scale $D = 1$. In CT-QMC calculations we vary I_z at fixed Γ_0, and are able to reach sufficiently low temperatures to access the asymptotic quantum critical regime. We fix I_z and vary Γ_0 when applying the NRG, a technique that can reach arbitrarily close to absolute zero but has limited ability to calculate finite-temperature dynamics. Further numerical details are described in the Supplemental Material [27].

Quantum critical properties: A critical phase boundary can be mapped out within the NRG by looking for the hybridization width $\Gamma_c(I_z)$ at which the asymptotic

low-energy many-body spectrum jumps from that of one stable fixed point to another. The phase boundaries for our two representative cases are plotted Fig. 1(b). For Γ_0 close to Γ_c, the NRG spectrum flows away from the critical spectrum toward one or other of the stable fixed points around a crossover temperature $T^* \propto |\Gamma_0 - \Gamma_c|^{\nu}$. Using this relation, illustrated in Fig. 1(c), one obtains $\nu^{-1} = 0.334(2)$ for $r = 0.2$ and $\nu^{-1} = 0.1835(4)$ for $r = 0.4$.

To search for a QCP using CT-QMC, we examine the Binder ratio $B(\beta, I_z)$ [28] defined as $B(\beta, I_z) = \langle M^4\rangle/\langle M^2\rangle^2$, where the staggered impurity magnetization $M = \beta^{-1}\int_0^\beta d\tau\,[S_1^z(\tau) - S_2^z(\tau)]$. Plots of $B(\beta, I_z)$ vs I_z for different values of $\beta = 1/k_BT$ should all cross at the location $I_z = I_c$ of any QCP, as is indeed shown in Fig. 2(a) for $r = 0.2$ and Fig. 2(b) for $r = 0.4$. A scaling collapse of the form

$$B(\beta, I_z) = f\left(\beta^{1/\nu}(I_z - I_c)/I_c + C\beta^{-\phi/\nu}\right) \qquad (3)$$

(where the term involving C accounts for sub-leading finite temperature corrections) demonstrates that the quantum phase transition at $I_z = I_c$ is second order, as illustrated in Fig. 2(c). By minimizing the quality function $S(I_c, \nu^{-1})$ [29] (see [27] for details), we find the reciprocal correlation-length exponent to be $\nu^{-1} = 0.33(4)$ for $r = 0.2$ and $\nu^{-1} = 0.20(2)$ for $r = 0.4$, reproducing the corresponding values from the NRG to within estimated errors [30].

The static staggered local spin susceptibility (the order-parameter susceptibility), defined as $\chi_z = \beta\langle M^2\rangle$, diverges at the QCP as

$$\chi_z(I_z = I_c, T) \sim T^{-x}, \qquad (4)$$

as seen in Fig. 2(d). The values of $x(r)$ from CT-QMC [$x(0.2) = 0.78(4)$ and $x(0.4) = 0.34(5)$] and the NRG [$x(0.2) = 0.78588(3)$ and $x(0.4) = 0.35075(3)$] are in good agreement. We have also calculated the connected spin susceptibility, $\chi_z^c = \beta(\langle M^2\rangle - \langle|M|\rangle^2)$, which based on the scaling hypothesis can be described by $\chi_z^c(\beta, I_z) = \beta^x g\left(\beta^{1/\nu}(I_z - I_c)\right)/I_c + C\beta^{-\phi/\nu})$; see plots in [27]. The estimated values of I_c, ν^{-1}, and x are all consistent with those reported above.

We summarize our results for the critical exponents ν^{-1} and x at the two-impurity pseudogap QCP CR2 in Table I, where we have also included NRG values of the order-parameter critical exponent β defined through $M(\Gamma_0, T = 0, h = 0) \propto (\Gamma_c - \Gamma_0)^{\beta}$ and the magnetic critical exponent $1/\delta$ defined through $M(\Gamma_0 = \Gamma_c, T = 0, h) \propto |h|^{1/\delta}$, h being an external field that couples solely to the staggered impurity spin (see plots in [27]). These exponents take values different from those at the single-impurity pseudogap QCP CR1 [16], demonstrating that CR2 represents a distinct critical point. Moreover, they obey scaling relations $\delta^{-1} = (1 - x)/(1 + x)$ and $\nu^{-1} = (1 - x)/2\beta$ expected to hold at an interacting critical point [16].

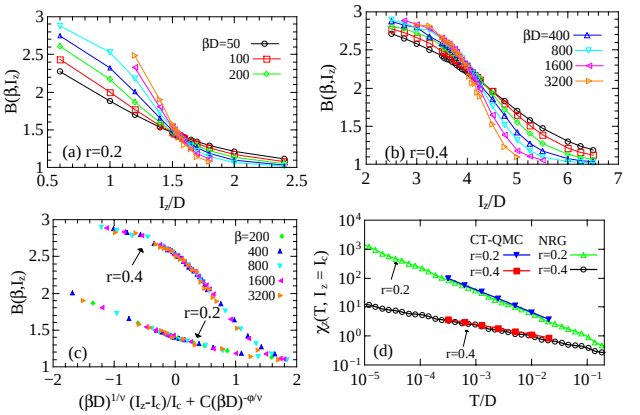

FIG. 2. (a,b) Binder ratio $B(\beta, I_z)$ from CT-QMC vs I_z at various inverse temperatures β for (a) $r = 0.2$, $\Gamma_0 = 0.5$ and (b) $r = 0.4$, $\Gamma_0 = 1.5$. (c) Scaling collapses of data in (a) giving $I_c = 1.56(7)$, $\nu^{-1} = 0.33(4)$ and of data in (b) giving $I_c = 3.75(7)$, $\nu^{-1} = 0.20(2)$. (d) Static staggered local spin susceptibility χ_z vs T at the estimated location $I_z = I_c$ of the QCP, calculated using CT-QMC and the NRG. Fitting to Eq. (4) yields the values of x given in the text.

We turn to the dynamical properties at CR2 of the single-particle Green's function $G_{i,\sigma}(\tau, T) = \langle T_\tau d_{i,\sigma}^\dagger(\tau)\, d_{i,\sigma}\rangle$ and the spin correlation function $\chi_z(\tau, T) = \langle T_\tau[S_1^z(\tau) - S_2^z(\tau)](S_1^z - S_2^z)\rangle$. Guided by previous work on the single-impurity models [13–15, 17], we find from CT-QMC (see [27]) that these functions share similar power-law forms in the low-T, large-τ limit:

$$G_{i,\sigma}(\tau, T) \sim [\pi T/\sin(\pi\tau T)]^{\eta_G(r)}, \qquad (5)$$

$$\chi_z(\tau, T) \sim [\pi T/\sin(\pi\tau T)]^{\eta_\chi(r)}, \qquad (6)$$

with exponents $\eta_G(0.2) = 0.795$, $\eta_G(0.4) = 0.600$, $\eta_\chi(0.2) = 0.213$, and $\eta_\chi(0.4) = 0.657$. As expected, $\eta_\chi = 1 - x$ is satisfied within numerical accuracy. Moreover, our results suggest that (i) the relation $\eta_G = 1 - r$ known to hold at CR1 [31] also applies at CR2, and (ii) $0 < \eta_G < 1$ and $0 < \eta_\chi < 1$, so $G_{i,\sigma}$ and χ_z will also obey ω/T scaling on the real frequency axis [17]. This supports the conclusion that CR2 is an interacting critical point.

Pairing susceptibilities: We study static pairing susceptibilities $\chi_\alpha(\beta, I_z) = \int_0^\beta d\tau\langle T_\tau\Delta_\alpha^\dagger(\tau)\,\Delta_\alpha\rangle$ with $\Delta_d = (d_{2\downarrow}d_{1\uparrow} - d_{2\uparrow}d_{1\downarrow})/\sqrt{2}$ (singlet channel) [32] and $\Delta_p =$

r	source	$1/\nu$	x	β	$1/\delta$
0.2	CT-QMC	0.33(4)	0.78(4)		
	NRG	0.334(2)	0.78588(3)	0.31991(2)	0.11990(4)
0.4	CT-QMC	0.20(2)	0.34(5)		
	NRG	0.1835(4)	0.35075(3)	1.7701(2)	0.48066(4)

TABLE I. Critical exponents (defined in the text) at the two-impurity pseudogap QCP CR2. Parentheses enclose the estimated error in the last decimal place.

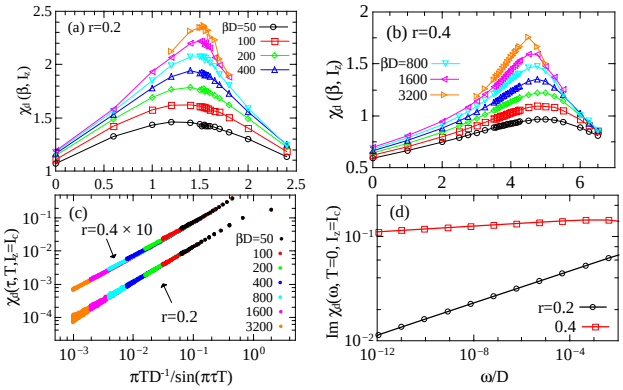

FIG. 3. Singlet pairing susceptibility: (a,b) static susceptibility $\chi_d(\beta, I_z)$ vs I_z at various inverse temperatures β for (a) $r = 0.2$, $\Gamma_0 = 0.5$, and (b) $r = 0.4$, $\Gamma_0 = 1.5$. (c) Imaginary-time susceptibility $\chi_d(\beta, \tau)$ at $I_z = I_c$, consistent with a $1/\tau^{1+y}$ decay with $y = 0.075$ for $r = 0.2$, $\Gamma_0 = 0.5$ and $y = 0.012$ for $r = 0.4$, $\Gamma_0 = 1.5$. (d) NRG results for the imaginary part of the real-frequency susceptibility, $\mathrm{Im}\,\chi_d(\omega) \propto \omega^y$, at $\Gamma_0 = \Gamma_c$, $T = 0$, calculated both for $r = 0.2$, $I_z = 1.54$ yielding $y = 0.077(1)$ and for $r = 0.4$, $I_z = 0.73$ yielding $y = 0.0139(1)$.

$(d_{1\uparrow}d_{2\uparrow} + d_{1\downarrow}d_{2\downarrow})/\sqrt{2}$ (triplet channel). Using the general four-point correlation function formula in CT-QMC [33], we find singlet pairing to be significantly enhanced near the QCP, as shown in Figs. 3(a) and 3(b). By contrast, triplet pairing is monotonically suppressed as I_z increases (see plots in [27]).

At $T = 0$, the imaginary part of the dynamical pairing susceptibility $\mathrm{Im}\,\chi_d(\omega)$ can be calculated using the NRG. We plot data for $\Gamma_0 = \Gamma_c(I_z)$ in Fig. 3(d) and for other cases in [27]. Our results can be summarized in the form

$$\mathrm{Im}\,\chi_d(\omega)\,\mathrm{sgn}(\omega) \propto \begin{cases} |\frac{\omega^*}{D}|^y |\frac{\omega}{\omega^*}|^{1-2r} & |\omega| < \omega^*, I_z < I_c \\ |\frac{\omega^*}{D}|^y |\frac{\omega}{\omega^*}|^{1+2r} & |\omega| < \omega^*, I_z > I_c \\ |\frac{\omega}{D}|^y & \omega^* < |\omega| < \omega_1, \end{cases} \tag{7}$$

where ω_1 is the high-energy scale marking the upper bound of the quantum critical regime and $\omega^* \simeq T^*$ is the scale for crossover into the low-temperature phase. This implies that at the critical point, $\chi_d(\tau) \sim 1/\tau^{1+y}$, cf. Fig. 3(c). The NRG gives $y = 0.077(1)$ for $r = 0.2$ and $y = 0.0139(1)$ for $r = 0.4$, values that agree very well with the CT-QMC estimates of $y = 0.075$ and $y = 0.012$, respectively. Equation (7) also implies (see [27]) that near the QCP,

$$\mathrm{Re}\,\chi_d(\omega = 0) = C_1(r) - C_2(r)\left(\frac{1}{y} - \frac{1}{1 \pm 2r}\right) \times \left(\frac{|(I_z - I_c)/I_c|^\nu}{D}\right)^y \tag{8}$$

with $\pm$ corresponding to $I_z > I_c$ or $I_z < I_c$, and $C_1(r)$ and $C_2(r)$ being independent of I_z. Given that $y\nu \ll 1$, $\mathrm{Re}\,\chi_d(\omega = 0)$ should have a pronounced cusp at $I_z = I_c$, as confirmed by the numerical data in Figs. 3(a) and 3(b).

Discussion and Summary: We now remark on several points. First, in the single-impurity pseudogap Anderson model, the impurity spectral function vanishes/diverges as $|\omega|^{\pm r}$ in the local-moment/Kondo-screened phase [34], corresponding to $G(\tau) \sim 1/\tau^{1\pm r}$ for $I_z > I_c$ or $I_z < I_c$. Our calculations suggest that this property also holds in the current two-impurity model (see [27]). This indicates that the frequency dependences of $\mathrm{Im}\,\chi_d(\omega)$ at the Kondo-screened and local-moment fixed points do not acquire any singular correction [21]. By contrast, the $1/\tau^{1+y}$ dependence of the singlet pairing correlation function at $I_z = I_c$ reflects the relevance of vertex corrections at an interacting critical point. Since CR1 and CR2 both exist only for $0 < r < \frac{1}{2}$, we expect that y is always smaller than $1 \pm 2r$ and that as $r \to \frac{1}{2}$, y and $1 - 2r$ both approach 0 before CR1 and CR2 merge with the Kondo-singlet fixed point and disappear. We therefore conclude that pairing fluctuations are always strongest in the quantum critical regime. This demonstrates that the underlying Kondo-destruction QCP promotes singlet superconducting pairing.

Second, we return to the issue raised earlier of the extent to which different kinds of magnetic interactions induce pairing correlations in non-Fermi liquid settings. Compared to the Ising-anisotropic Bose-Fermi Anderson model [20], the interactions that induce Kondo destruction in the pseudogapped Anderson model are spin isotropic; note that the decoupled impurity problem at CR1 has SU(2) symmetry. Even though the problem is no longer fully SU(2) invariant at the fixed point CR2, the spin-flip fluctuations are still enhanced, as observed from the transverse component of the spin susceptibility $\chi_{+-}(\tau)$ having a slower power-law decay compared to its tree-level form (see [27]). This implies that our model has strong correlations in the spin-singlet channel. Consistent with general considerations, our results demonstrate that the superconducting pairing correlations in the singlet channel are much stronger here than in the Ising-anisotropic two-impurity Bose-Fermi Anderson model.

To summarize, we have found a quantum critical point in the two-impurity Anderson model with a pseudogap density of states. It exhibits critical Kondo destruction and shows all the hallmarks of an interacting fixed point, such as hyperscaling relations among critical exponents and ω/T scaling in the dynamical properties. The singlet pairing susceptibility is found to be sharply peaked at the quantum critical point. Our results elucidate how different kinds of magnetic interactions promote spin-singlet pairing correlations in non-Fermi liquid settings, and provide the basis for understanding superconductivity in the Kondo-destruction quantum critical heavy-fermion systems such as $CeRhIn_5$.

Acknowledgements. We acknowledge useful discussions with Y. Chou, E. M. Nica, S. Kirchner, Z. Wang, and

H. Xie, as well as technical support from the Center for Research Computing at Rice University. This work was supported in part by NSF Grant No. DMR-1309531 and the Robert A. Welch Foundation Grant No. C-1411 (A.C. and Q.S.), by JQI-NSF-PFC, LPS-MPO-CMTC and Microsoft Q (J.H.P.), and by NSF Grants No. DMR-1107814 and No. DMR-1508122 (K.I.). The computation was mainly performed on the Shared Computing Infrastructure funded by NSF under grant OCI-0959097, NIH award NCRR S10RR02950, and an IBM Shared University Research (SUR) Award in partnership with CISCO, Qlogic and Adaptive Computing, and Rice University.

[1] Q. Si and F. Steglich, Science **329**, 1161 (2010).
[2] H. Löhneysen, A. Rosch, M. Vojta, and P. Wölfle Rev. Mod. Phys. **79**, 1015, (2007).
[3] J. A. Hertz, Phys. Rev. B **14**, 1165 (1976).
[4] A. J. Millis, Phys. Rev. B **48**, 7183 (1993).
[5] T. Moriya *Spin Fluctuations in Itinerant Electron Magnetism*, **56**, 44–81 (Springer, 1985).
[6] Q. Si, S. Rabello, K. Ingersent, and J. L. Smith, Nature **413**, 804 (2001).
[7] P. Coleman, C. Pépin, Q. Si, and R. Ramazashvili, J. Phys.: Condens. Matter **13**, R723 (2001).
[8] T. Park, F. Ronning, H. Q. Yuan, M. B. Salamon, R. Movshovich, J. L. Sarrao, and J. D. Thompson, Nature **440**, 65 (2006).
[9] T. Park, E. D. Bauer, and J. D. Thompson Phys. Rev. Lett. **101**, 177002 (2008).
[10] O. Stockert, S. Kirchner, F . Steglich, Q. Si, J. Phys. Soc. Jpn. **81**, 011001 (2012).
[11] Q. Si, J. H. Pixley, E. Nica, S. J. Yamamoto, P. Goswami, R. Yu, and S. Kirchner, J. Phys. Soc. Jpn. **83**, 061005 (2014).
[12] H. Shishido, R. Settai, H. Harima, and Y. Ōnuki, J. Phys. Soc. Jpn. **74**, 1103 (2005).
[13] J. H. Pixley, S. Kirchner, K. Ingersent, and Q. Si, Phys. Rev. B **88**, 245111 (2013).
[14] S. Kirchner and Q. Si, Phys. Rev. Lett. **100**, 026403 (2008).
[15] J. H. Pixley, S. Kirchner, K. Ingersent, and Q. Si, Phys. Rev. Lett. **109**, 086403 (2012).
[16] K. Ingersent and Q. Si, Phys. Rev. Lett. **89**, 076403 (2002).
[17] M. T. Glossop, S. Kirchner, J. H. Pixley, and Q. Si, Phys. Rev. Lett. **107**, 076404 (2011).
[18] J. H. Pixley, A. Cai and Q. Si, Phys. Rev. B **91**, 125127 (2015).
[19] J. H. Pixley, T. Chowdhury, M. T. Miecnikowski, J. Stephens, C. Wagner, and K. Ingersent, Phys. Rev. B **91**, 245122 (2015).
[20] J. H. Pixley, L. Deng, K. Ingersent, and Q. Si, Phys. Rev. B **91**, 201109(R) (2015).
[21] C. Gonzalez-Buxton, and K. Ingersent, Phys. Rev. B **57**, 14254 (1998).
[22] In the absence of the pseudogap, our model exhibits a Kosterlitz-Thouless quantum phase transition between Kondo and Kondo-destroyed phases; see M. Garst, S. Kehrein, T. Pruschke, A. Rosch, and M. Vojta, Phys. Rev. B **69**, 214413 (2014), also N. Garst, G. T. Zimányi, G. Schön, Phys. Rev. B **60**, R5125 (1999).
[23] P. Werner and A. J. Millis, Phys. Rev. Lett. **99**, 146404 (2007).
[24] P. Werner and A. J. Millis, Phys. Rev. Lett. **104**, 146401 (2010).
[25] K. G. Wilson, Rev. Mod. Phys. **47**, 773 (1975).
[26] R. Bulla, T. A. Costi, and T. Pruschke, Rev. Mod. Phys. **80**, 395 (2008).
[27] See Supplemental Material at http://
[28] K. Binder, Z. Phys. B **43**, 119 (1981).
[29] J. Houdayer and A. K. Hartmann, Phys. Rev. B **70**, 014418 (2004).
[30] For $r = 0.4$, sub-leading corrections to scaling are sufficiently strong that it proved challenging for CT-QMC to reproduce the NRG value of ν^{-1} within estimated error. We attained this goal by using NRG calculations to select the value $\Gamma_0 = 1.5$ that produces the highest temperature of entry into the quantum critical regime.
[31] M. Kirćan, and M. Vojta, Phys. Rev. B **69**, 174421 (2004).
[32] We note that in the infinite-separation limit, the pairing correlation of $d_{2\downarrow}d_{1\uparrow} + d_{2\uparrow}d_{1\downarrow}$ is degenerate with that of $d_{2\downarrow}d_{1\uparrow} - d_{2\uparrow}d_{1\downarrow}$.
[33] E. Gull, P. Werner, A. Millis, and M. Troyer, Phys. Rev. B **76**, 235123 (2007).
[34] R. Bulla, T. Pruschke, and A. C. Hewson, J. Phys.: Condens. Matter **9**, 10463 (1997).

SUPPLEMENTAL MATERIAL

by: Ang Cai, J. H. Pixley, Kevin Ingersent, and Qimiao Si

Methods

The CT-QMC hybridization expansion algorithm allows us to stochastically sample the perturbation series in the hybridization term free of any sign problem in the infinite separation limit. The average perturbation order exceeds 10^3 per orbital for the largest inverse temperature, $\beta = 3200$ at $\Gamma_0 = 1.5$. Within our specific case, we find the auto-correlation time measured in terms of successful updates will grow not only as temperature is lowered and perturbation order increases, but also as one increases I_z deep into the magnetic ordered phase, where a domain wall like structure can form in the imaginary time direction. Therefore, we have introduced an additional global update in addition to the standard local one kink (a kink refers to a creation and annihilation operator pair) and two kinks update, by exchanging all the kinks between different orbitals within a imaginary time interval of length around $\beta/2$ (with a probability that satisfies detailed balance), to prevent the sampling process from getting trapped in some meta-stable state.

The NRG runs were performed for Wilson discretization parameter $\Lambda = 9$, retaining between 1000 and 4000 many-body eigenstates after each iteration. The Wilsonian discretization of the conduction band reduces the effective density of states so it is appropriate to compare NRG calculations for hybridization width Γ_0 with continuum-limt ($\Lambda \to 1$) results for hybridization width $\Gamma_0/A(\Lambda, r)$, where $A(\Lambda, r)$ is defined in Ref. 21 of the main text. Hybridization widths reported in the text are the values entered into the NRG calculations and do not include the discretization correction factor.

Finite Size Scaling of Binder Cumulant

The value of ν^{-1} and I_c is determined through minimization of the quality function $S(I_c, \nu^{-1})$, which is essentially the mean square deviation of the scaled data points with respect to the unknown universal function. For k sets of data points represented by $\{x_{ij}, y_{ij}\}$, where $i = 1, \cdots, k$ labels different β and j labels different I_z, we define $S(I_c, \nu^{-1}) = 1/N \sum_{i,j}(y_{ij} - Y_{ij})^2$. Here Y_{ij} is the estimated value of the universal function at x_{ij} by linear interpolation from the rest of sets $\{x_{i'j}, y_{i'j}\}$, $i' \neq i$. During the scaling collapse, we start by including all the sets, and then gradually excluding the highest temperature data until the result reaches convergence. Only data points satisfying $\beta^{1/\nu}(I_z - I_c)/I_c \lesssim 1$ are included. The best estimate of I_c and ν^{-1} is where $S(I_c, \nu^{-1})$ reaches its minimum S_{min}. We estimate the error by requiring $S(I_c + \delta I_c, \nu^{-1} + \delta\nu^{-1}) - S_{min} \simeq S_{min}/2$.

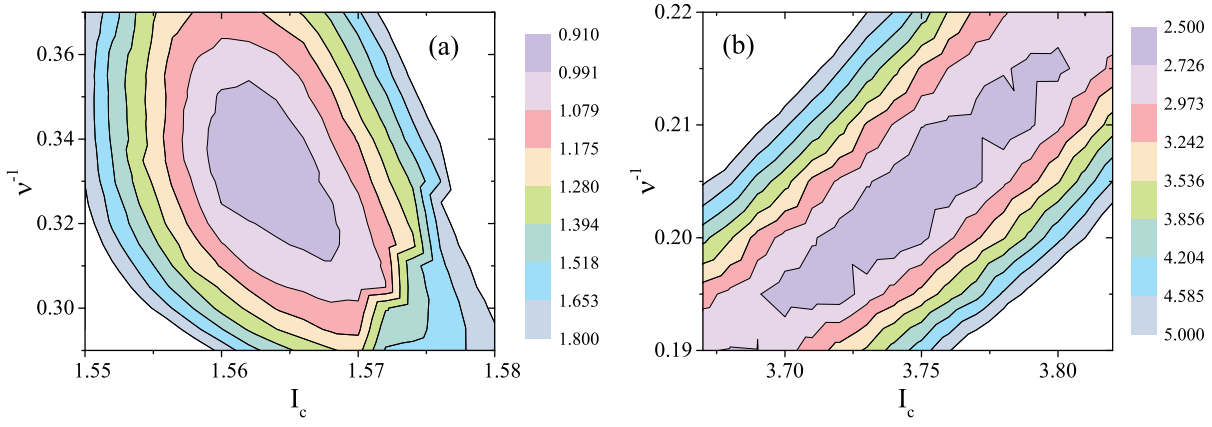

FIG. S1. Contour plot of quality function $S(I_c, \nu^{-1}) \times 10^4$ for the scaling collapse shown in Fig. 2(c) for (a) $r = 0.2$ and (b) $r = 0.4$.

Additional data from CT-QMC

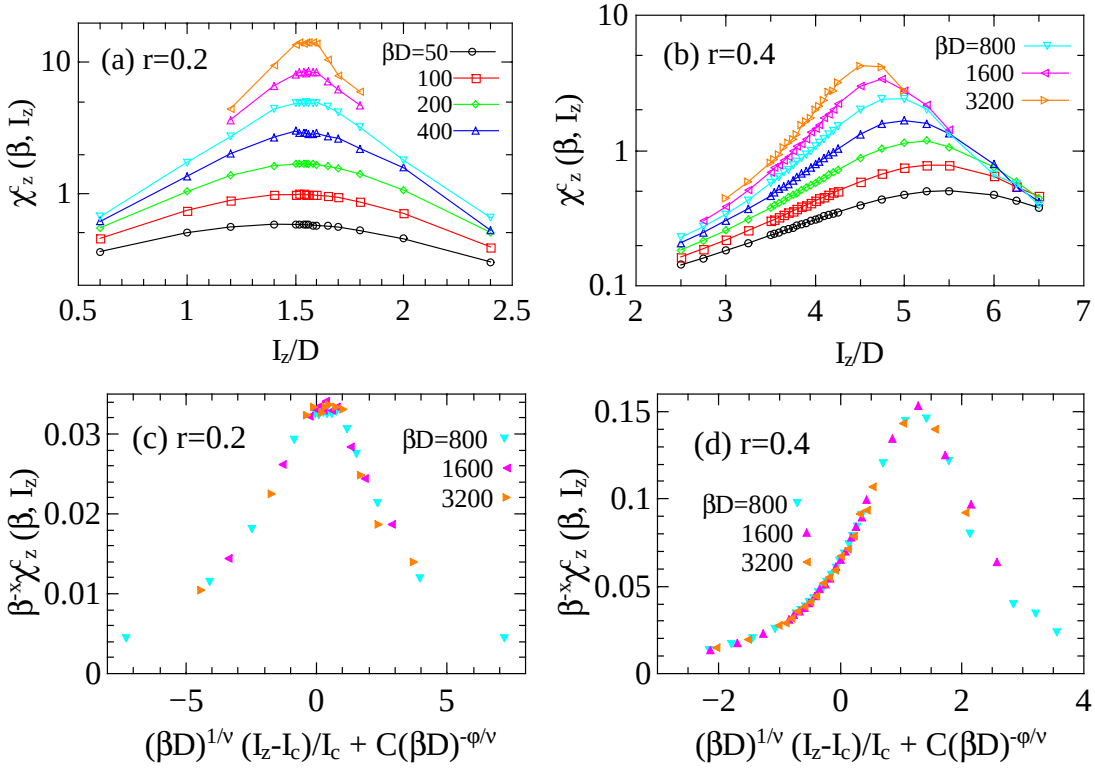

FIG. S2. Connected static staggered spin susceptibility $\chi^c_z(\beta, I_z)$ vs I_z at various inverse temperatures β for (a) $r = 0.2$, $\Gamma_0 = 0.5$ and (b) $r = 0.4$, $\Gamma_0 = 1.5$. (c)(d) Scaling collapse of $\chi^c_z(\beta, I_z)$ in (a) and (b) respectively, with $I_c = 1.53(6)$, $\nu^{-1} = 0.37(8)$, $x = 0.75(4)$ at $r = 0.2$ and $I_c = 4.0(2)$, $\nu^{-1} = 0.26(4)$, $x = 0.42(7)$ at $r = 0.4$. The deviation from exponents in Table I can be attributed to stronger finite-size corrections to χ^c_z.

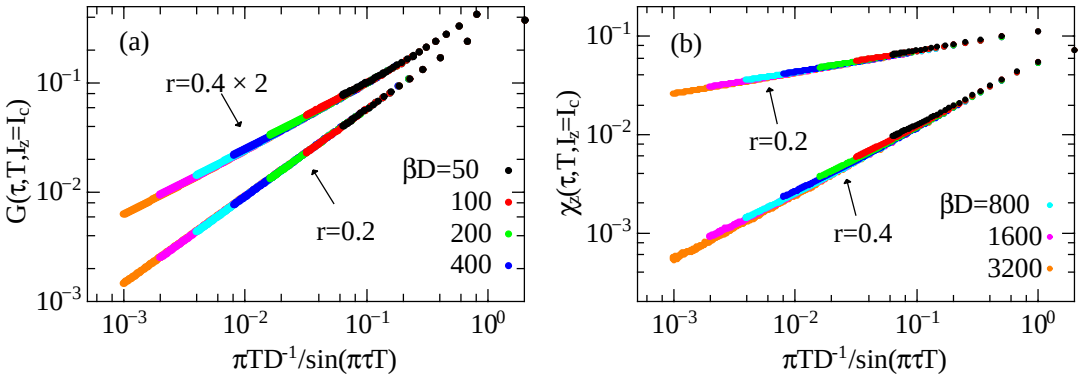

FIG. S3. (a) Scaling of the single-particle Green's function $G(\tau, T, I_z = I_c)$ (averaged over impurity site and spin) with $\pi T/\sin(\pi\tau T)$. We find $G(\tau \to \infty, T \to 0, I_z = I_c) \sim [\pi T/\sin(\pi\tau T)]^{\eta_G(r)}$ with $\eta_G(0.2) = 0.795$ and $\eta_G(0.4) = 0.600$, consistent with $\eta_G = 1 - r$ (b) Scaling of the staggered spin correlation function $\chi_z(\tau, T, I_z = I_c)$ with $\pi T/\sin(\pi\tau T)$. We find $\chi_z(\tau \to \infty, T \to 0, I_z = I_c) \sim [\pi T/\sin(\pi\tau T)]^{\eta_\chi(r)}$ with $\eta_\chi(0.2) = 0.213$ and $\eta_\chi(0.4) = 0.657$, consistent with $\eta_\chi = 1 - x$. Calculations are performed at $\Gamma_0 = 0.5$ at $r = 0.2$ and $\Gamma_0 = 1.5$ at $r = 0.4$.

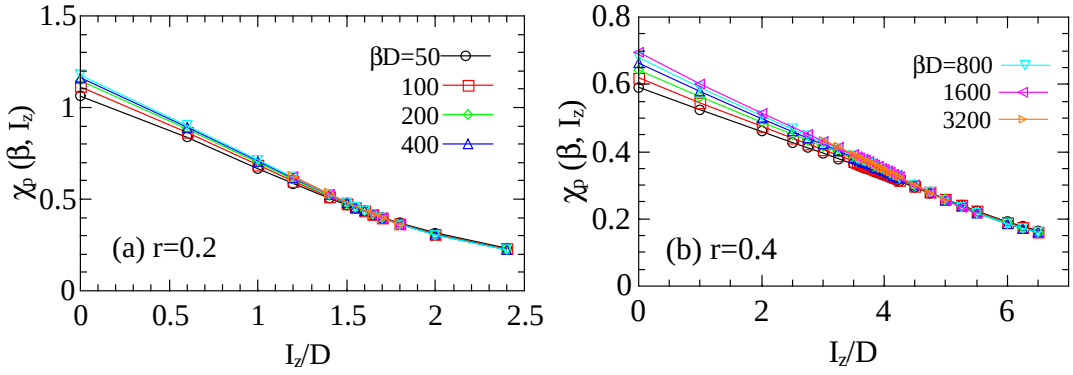

FIG. S4. Static triplet pairing susceptibility $\chi_p(\beta, I_z)$ vs I_z at various inverse temperatures β for (a) $r = 0.2$, $\Gamma_0 = 0.5$ and (b) $r = 0.4$, $\Gamma_0 = 1.5$.

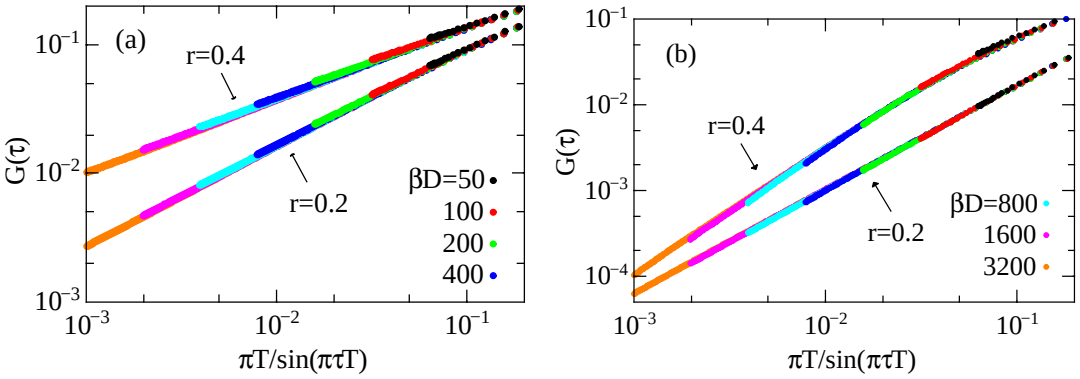

FIG. S5. Single-impurity Green's function $G(\tau, T)$ in (a) the Kondo-screened phase ($I_z = 0$, $\Gamma_0 = 0.5$ for both $r = 0.2$ and $r = 0.4$) and (b) the local-moment phase ($I_z = 3$, $\Gamma_0 = 0.5$ for $r = 0.2$ and $I_z = 2$, $\Gamma_0 = 0.5$ for $r = 0.4$). Fitting to $G_{i,\sigma}(\tau, T) \sim [\pi T/\sin(\pi\tau T)]^{\eta_G(r)}$ over $I_z < I_c$ gives $\eta_G(0.2) = 0.77$ and $\eta_G(0.4) = 0.57$, while fitting over $I_z > I_c$ gives $\eta_G(0.2) = 1.21$ and $\eta_G(0.4) = 1.45$. Results are consistent with $G(\tau) \sim 1/\tau^{1\pm r}$ for $I_z > I_c$ or $I_z < I_c$.

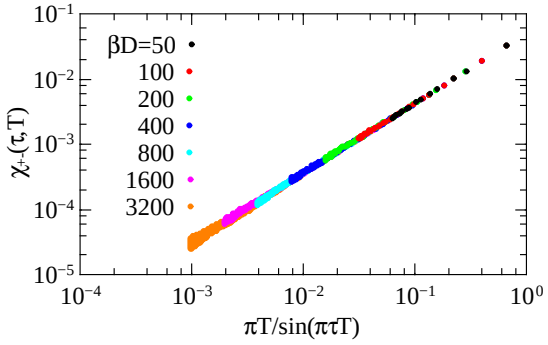

FIG. S6. Transverse component of the staggered spin susceptibility $\chi_{+-}(\tau)$ at $I_z = I_c$, $\Gamma_0 = 0.5$ for $r = 0.2$. $\chi_{+-}(\tau) = \int_0^\beta d\tau \langle T_\tau \frac{1}{2}(S_1^+(\tau) - S_2^+(\tau))\frac{1}{2}(S_1^- - S_2^-)\rangle/2$, with $S_i^- = d_{i\downarrow}^\dagger d_{i\uparrow}$ and $S_i^+ = S_i^{-\dagger}$, such that $\chi_z = \chi_{+-}$ at the $I_z = 0$ SU(2)-symmetric point. The result is consistent with $\chi_{+-}(\tau) \sim 1/\tau^{1+y}$, with y taking the same value (within numerical uncertainty) as found in the singlet pairing susceptibility $\chi_d(\tau)$.

Additional data from NRG

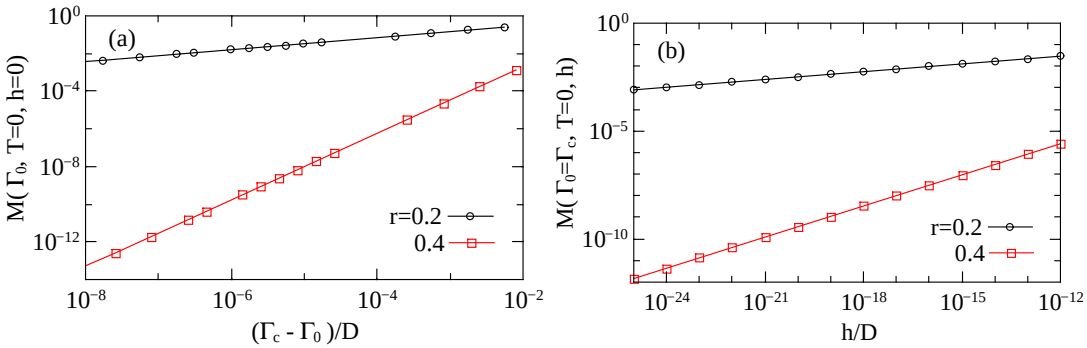

FIG. S7. (a) Staggered local moment $M(\Gamma_0, T=0, h=0)$ vs $\Gamma_c - \Gamma_0$, fitted to $M \propto (\Gamma_c - \Gamma_0)^\beta$ with $\beta = 0.31991(2)$ for $r = 0.2$ and $\beta = 1.7701(2)$ for $r = 0.4$. (b) Staggered local moment $M(\Gamma_0 = \Gamma_c, T=0, h)$ vs staggered external magnetic field h, fitted to $M \propto h^{1/\delta}$ with $1/\delta = 0.11990(4)$ for $r = 0.2$ and $1/\delta = 0.48066(4)$ for $r = 0.4$. Calculations are performed at $I_z = 1.54\,(0.73)$ for $r = 0.2$ (0.4).

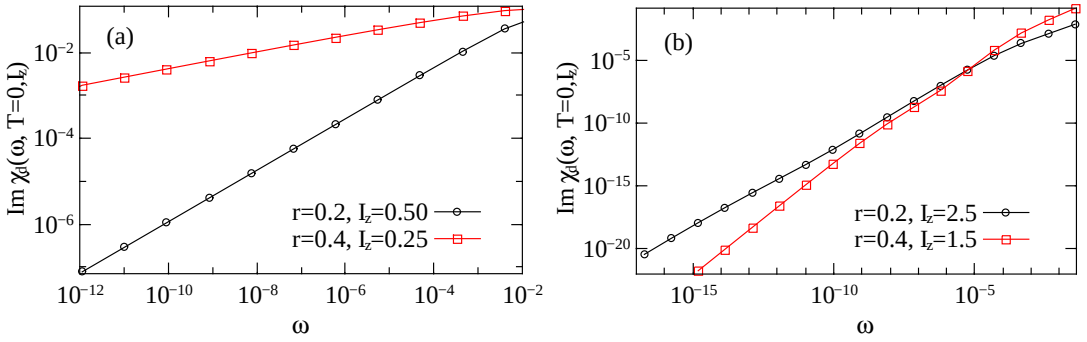

FIG. S8. $\mathrm{Im}\,\chi_d(\omega)$ at $T = 0$ in (a) Kondo-screened and (b) local-moment phases. The low-frequency asymptotics give (a) $\mathrm{Im}\,\chi_d(\omega)\,\mathrm{sgn}(\omega) \propto |\omega|^{1-2r}$ and (b) $\mathrm{Im}\,\chi_d(\omega)\,\mathrm{sgn}(\omega) \propto |\omega|^{1+2r}$. Calculations are performed at $\Gamma_0 = 0.5503$ and $\Gamma_0 = 0.8032$, respectively.

Derivation of Eq. (8)

We make use of the Kramers-Kronig relation

$$\mathrm{Re}\,\chi_d(\omega = 0) = \frac{1}{\pi}\int_{-\infty}^{\infty} d\omega' \frac{\mathrm{Im}\,\chi_d(\omega')}{\omega'}. \tag{S1}$$

Because $\mathrm{Im}\,\chi_d(\omega')$ is odd,

$$\mathrm{Re}\,\chi_d(\omega = 0) = \frac{2}{\pi}\int_0^{\infty} d\omega \frac{\mathrm{Im}\,\chi_d(\omega)}{\omega} \tag{S2}$$

$$= \frac{2}{\pi}\Big(\int_0^{\omega^*} d\omega + \int_{\omega^*}^{\omega_1} d\omega + \int_{\omega_1}^{\infty} d\omega\Big)\frac{\mathrm{Im}\,\chi_d(\omega)}{\omega}, \tag{S3}$$

where $\omega^* \sim |(I_z - I_c)/I_c|^\nu$ is the crossover scale into the quantum critical regime, and ω_1 is some upper cutoff, which we have assumed to be independent of I_z. The high-frequency non-universal part should only have a weak dependence on I_z, so we put $\int_{\omega_1}^{\infty} d\omega\,[\mathrm{Im}\,\chi_d(\omega)]/\omega \simeq D_1(r)$.

Now we substitute Eq. (7) in the main text.

$$\mathrm{Re}\,\chi_d(\omega=0) = \frac{2}{\pi}\int_0^{\omega^*} C\left(\frac{\omega^*}{D}\right)^y \left(\frac{\omega}{\omega^*}\right)^{1\pm 2r}\frac{1}{\omega}d\omega + \frac{2}{\pi}\int_\omega^{\omega_1} C\left(\frac{\omega^*}{D}\right)^y \frac{1}{\omega}d\omega + D_1(r) \tag{S4}$$

$$= \frac{2}{\pi}C\left(\frac{\omega^*}{D}\right)^y \frac{1}{1\pm 2r} + \frac{2}{\pi}C\frac{1}{y}\frac{(\omega_1^y - \omega^{*y})}{D^y} + D_1(r) \tag{S5}$$

$$= \frac{2C}{\pi}\left[\frac{1}{y}\frac{\omega_1^y}{D^y} - \left(\frac{\omega^*}{D}\right)^y\left(\frac{1}{y} - \frac{1}{1\pm 2r}\right)\right] + D_1(r) \tag{S6}$$

From NRG data, the proportionality constant C has negligible dependence on I_z. Finally we replace ω^* by $|(I_z - I_c)/I_c)|^\nu$ to obtain

$$\mathrm{Re}\,\chi_d(\omega=0) = C_1(r) - C_2(r)\left(\frac{1}{y} - \frac{1}{1\pm 2r}\right)\left(\frac{|(I_z - I_c)/I_z|^\nu}{D}\right)^y, \tag{S7}$$

where

$$C_1(r) = \frac{2C(r)}{\pi}\frac{1}{y}\frac{\omega_1^y}{D^y} + D_1(r), \quad C_2(r) = \frac{2C(r)}{\pi}. \tag{S8}$$